Title

Stabilization and control of persistent current magnets using variable inductance

Journal

Superconductor Science and Technology, 35(4)

ISSN

0953-2048

Authors

Brouwer, Lucas

Shen, Tengming

Norris, Ryan

et al.

Publication Date

2022-04-01

DOI

10.1088/1361-6668/ac549b

Stabilization and control of persistent current magnets using variable inductance

Lucas Brouwer[1], Tengming Shen[1], Ryan Norris[1,2], Aurelio Hafalia[1], Ross Schlueter[1], Li Wang[1], Jim Ciston[1], Peter Ercius[1], Qing Ji[1], Marian Mankos[3], Colin Ophus[1], Alexander Stibor[1], Andreas Schmid[1], Andrew M. Minor[1,2], and Peter Denes[1]

[1] Lawrence Berkeley National Laboratory, Berkeley, CA, 94720 USA
[2] University of California, Berkeley, CA, 94720 USA
[3] Electron Optica, Palo Alto, CA, 94303 USA

E-mail: lnbrouwer@lbl.gov

Abstract.

Ultra-stable, tunable magnetic fields are desirable for a wide range of applications in medical imaging, electron microscopy, quantum science, and atomic physics. Superconducting magnets operated in persistent current mode, with device current flowing in a closed superconducting loop disconnected from a power source, are a common approach for applications with the most stringent requirements on temporal field stability. We present a method for active control of this persistent current by means of dynamic inductance change within the superconducting circuit. For a first realization of this general technique, we consider a variable superconducting inductor placed in series with the main magnet. The inductor acts as a dynamic flux storage device capable of transferring flux to or from the main magnet through inductance change. This allows for fine and fast adjustments of the persistent current without the use of thermal switches that limit the speed and accuracy of many present-day methods. With first experiments employing this technique, we demonstrate stabilization of a 1.95 T Nb-Ti round lens for electron microscopy against decay resulting from residual losses in the superconducting circuit, and more generally show flexibility for precise control over the magnitude and waveform of the persistent current.

Submitted to: *Supercond. Sci. Technol. DOI: https://doi.org/10.1088/1361-6668/ac549b*

Keywords: superconducting magnets, persistent current, superconducting joints, medical imaging, cryogenic electron microscopy

1. Introduction

Magnetic fields of high temporal stability are required for many medical and scientific applications. In magnetic resonance imaging (MRI), one of the most prolific applications

of superconducting magnets, there are strict requirements on field drift typically near 0.01-0.1 parts per million (ppm) per hour. Field stability demands are even more extreme for electron microscopy and fundamental physics experiments employing Penning traps. To achieve the desired focal stability of one nanometer or better in electron microscopy, magnetic field fluctuations in the objective lens must reduced below the parts per billion (ppb) level. A similar level of stability is desired for precision measurements of atomic masses and fundamental constants with Penning traps. Present experiments in these areas are limited by magnetic field stability [1], motivating a large effort into the design and operation of ultra-stable superconducting magnet systems [2, 3, 4, 5, 6].

Superconducting magnets produce exceptionally stable magnetic fields when operating in persistent current mode, making them an attractive design choice for these ultra-stable applications. Persistent current mode is characterized by the magnet current flowing in a closed superconducting loop independent of a power source, and is traditionally established by means of a superconducting switch which removes the power supply from the magnet circuit after initialization of the current. Remaining field drift is dominated by small residual loss due to superconducting joint resistances and index loss within the superconductor itself. Nb-Ti to Nb-Ti superconducting joints are a mature technology with resistances of 10^{-12} Ω or lower routinely achievable [7]. This low resistance typically enables meeting the drift criteria for large inductance Nb-Ti MRI magnets without further stabilization. Emerging high-field MRI and other specialty magnets making use of high-temperature superconductors (HTS) require powered operation or persistent current stabilization techniques [8] due to larger joint resistances and increased index loss within the HTS material [9, 10].

Present-day electron microscopes employ resistive magnet technology operated at room temperature. These machines are stabilized using a combination of environmental control [11] and ultra-stable magnet power supplies [12], and achieve field stability on the order of 100 ppb in the objective magnetic lens. Operating the entire microscope at liquid helium temperature is a route to improve both environmental and magnet stability. This cooling greatly reduces thermal drift, enables superconducting electromagnetic shielding, enhances the vacuum environment, and allows for use of persistent current superconducting magnets [13]. The sub-ppb level of field stability desired for the low inductance magnets (several millihenries as opposed to tens or hundreds of henries for an MRI) cannot be achieved using only Nb-Ti joints and persistent current operation due to excessive drift. This further motivates the development of techniques that can stabilize the persistent current to prevent field drift.

Existing methods for field stabilization can be grouped into passive and active techniques. Passive methods typically employ a superconducting shield with a coil-specific geometry chosen to cancel field fluctuations in the region of interest [14, 15]. In active techniques, flux is transferred in and out of the superconducting loop by means of a flux pumping sequence [8, 16], enabling not only active stabilization, but also the ability to adjust the nominal value of the persistent current. Due to conservation of

flux linkage in superconducting circuits, most flux pumping schemes rely on strategies which break and close superconducting connections to move flux into the desired closed loop within the circuit. This quench and then recover sequence, particularly if driven by thermal processes, limits the speed and accuracy of persistent current adjustment.

In this paper, we present a method for active control of persistent current magnets by means of inductance change within the superconducting circuit. A simple realization of the concept is studied in which a variable, superconducting inductor is placed in series with the main magnet. At the point of initial powering, this inductor stores a certain amount of extra flux which can be transferred to and from the main coil by inductance change. This flux re-balancing can be used to stabilize the main coil against decay, adjust the level of persistent current, or add a waveform to the current. Because flux is not moved in or out of the superconducting loop, the accuracy and speed of tuning is decoupled from quench-based breaking of superconducting connections. We first give an overview of the basic operating principles of the technique. Then, the design of a tuning system using a cryogenic linear stage for fine control of a variable, superconducting inductor is presented. Finally, we report on first experiments integrating this tuning setup with a prototype Nb-Ti superconducting objective lens for electron microscopy. This testing demonstrates a level of control over the persistent current reaching the field measurement limit of the cryogenic hall probe technology employed (several ppm at 1.95 T).

2. Basic Principle

2.1. Idealized circuits with no loss

Inductance and current in closed, ideal superconducting circuits are coupled by conservation of flux linkage (a consequence of Faraday's law). In the idealized superconducting circuit shown in figure 1, a persistent current i flows in a closed, superconducting loop of inductance L, resulting in a flux of $\lambda = iL$. For this simple example, the circuit behavior is described by

$$L\frac{di}{dt} + i\frac{dL}{dt} = \frac{d\lambda}{dt} = 0. \tag{1}$$

If i_0 and L_0 are the initial persistent current and inductance, the current evolution as a function of time is

$$i(t) = \frac{i_0 L_0}{L(t)}, \tag{2}$$

which clearly illustrates how changes in circuit inductance can be used to adjust the level of the persistent current.

If two magnets are included in the circuit, the effect of inductance change in the individual magnets can be interpreted as a re-balancing of the total conserved flux. Figure 2 illustrates this process. In (a), the total flux λ_0 is split between the main

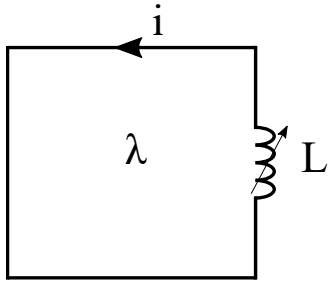

Figure 1. Conservation of flux linkage in idealized, closed superconducting circuits couples inductance and persistent current change.

magnet $\lambda_m = i_0 L_m$ and the tunable inductor $\lambda_b = i_0 L_b$ based on a balence of their inductance ratios. As illustrated in (b), a change in the inductance of the tuner causes the flux to re-balance. A reduction in tuner inductance shifts flux from the tuner to the main magnet with a net increase in the persistent current. If the tuner inductance is increased, the opposite occurs, and flux re-balances by shifting from the main magnet to the tuner (resulting in a drop of the persistent current level).

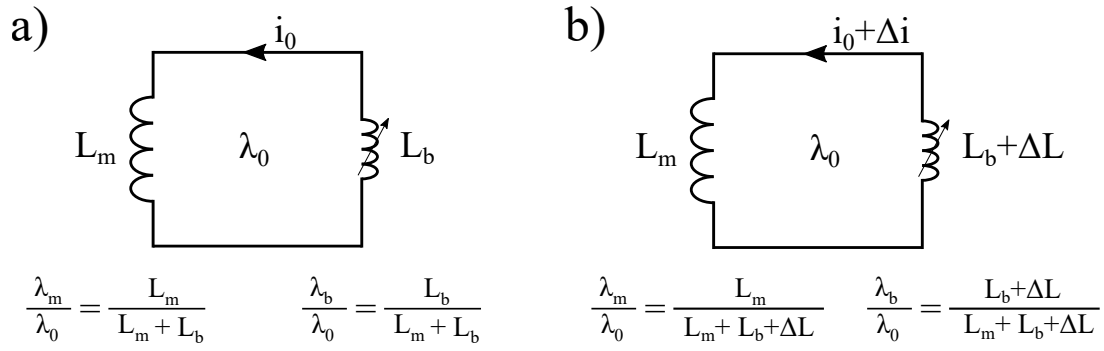

Figure 2. (a) A persistent current i_0 results in a total flux λ_0 that is balanced between the magnets based on their inductance ratios. (b) A change in the inductance of one magnet re-balances the conserved initial flux, adjusting the magnitude of the persistent current. If L_m is the main magnet, the extra flux stored in the tunable inductor L_b at initial powering can be shifted to the main magnet, or vice versa, without breaking the superconducting loop.

The percentage of the flux moved from the tuner to the main magnet for a given inductance change ΔL of the tuner is

$$\frac{\Delta\lambda_{b\to m}}{\lambda_0} = f_b\left(1 - \frac{1 + f_\Delta/f_b}{1 + f_\Delta}\right), \tag{3}$$

where the inductance fractions are defined as $f_b \equiv L_b/(L_m{+}L_b)$ and $f_\Delta \equiv \Delta L/(L_m{+}L_b)$. This results in a relative change of flux in the main magnet and tuner of

$$\frac{\Delta\lambda_m}{\lambda_m} = -\frac{f_\Delta}{1+f_\Delta} \tag{4}$$

$$\frac{\Delta\lambda_b}{\lambda_b} = \left(\frac{1-f_b}{f_b}\right)\frac{f_\Delta}{1+f_\Delta}, \tag{5}$$

and relative change in the persistent current of

$$\frac{\Delta i}{i_0} = -\frac{f_\Delta}{1+f_\Delta}, \tag{6}$$

which is consistent with equation 2 for a time independent step change.

2.2. Application to circuits with loss

To apply this concept to the operation of a typical persistent current magnet, we consider the circuit illustrated in figure 3. A resistive source of flux loss R is now included to capture the effects of superconducting joints and index loss within the superconductor itself. For simplicity, we also separate the source of inductance change within the circuit (a tunable inductor L_b) from the main superconducting magnet L_m. This isolates the impact of the inductance change from the magnetic field distribution or other important performance metrics of the main magnet.

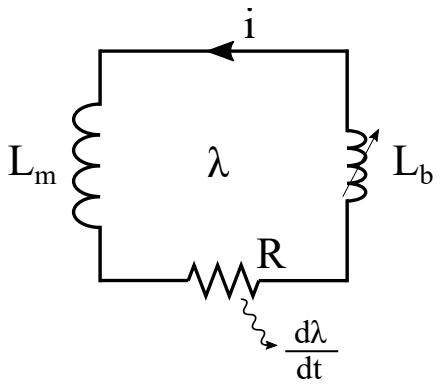

Figure 3. A tunable inductor L_b is placed in series with a main magnet L_m to control its operation through inductance change.

With these assumptions, the circuit behavior is governed by

$$(L_m + L_b)\frac{di}{dt} + i\frac{dL_b}{dt} + iR = 0. \tag{7}$$

If the inductance is fixed, the current in circuit will decay exponentially as $i(t) = i_0 e^{-t/\tau}$ with the time constant $\tau = (L_m + L_b)/R$. For many applications it is desirable to

stabilize the current in the loop against this decay. If the inductance L_b is allowed to vary in time, the required rate of inductance change for stabilization is simply

$$\frac{dL_b}{dt} = -R. \tag{8}$$

Critical metrics for the design of an inductance tuning system are the total time for which the current can be stabilized and the precision to which deviation of the current from a nominal value can be prevented. In practice, this is generally limited by the the total range over which the inductance can be varied and the minimum achievable change of inductance of the tuner. If $\Delta L_{b,max}$ is the maximum available change in tuner inductance, the time for which a system can be stabilized is

$$t_{stab} = -\frac{\Delta L_{b,max}}{R}. \tag{9}$$

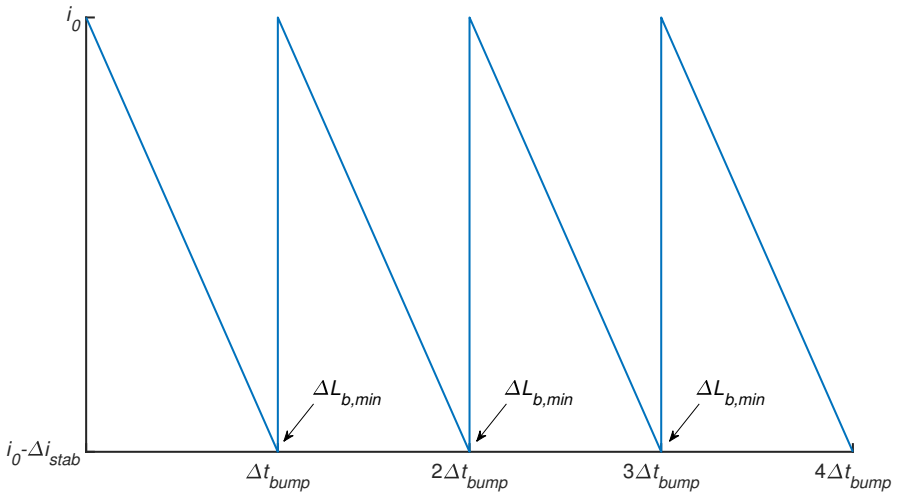

Figure 4. The minimum step change of the tuner inductance $\Delta L_{b,min}$ sets the reaction time Δt_{bump} and the theoretical limit to which the current can be stabilized of Δi_{stab}.

Figure 4 illustrates the behavior of the system during stabilization for typical magnet and tuner parameters. When the deviation of the current from the nominal value reaches the point of minimum adjustment

$$\frac{\Delta i_{stab}}{i_0} = -\frac{\Delta L_{b,min}/(L_m + L_b)}{\Delta L_{b,min}/(L_m + L_b) + 1}, \tag{10}$$

a minimum inductance change of the tuner $\Delta L_{b,min}$ is triggered to restore the current. In the limit of fast inductance change, this results in a sawtooth pattern with periodic bumping of the current. In many cases, the small change in tuner inductance will have a negligible effect on the decay time constant, resulting in a periodic time between bumps of

$$\Delta t_{bump} = -\tau \ln\left(\frac{\Delta i_{stab}}{i_0} + 1\right), \tag{11}$$

where a constant $\Delta L_{b,min}$ across the full range of tuner inductance is also assumed.

3. The magnet and tuning system

An overview of the magnet system is shown in figure 5. The primary element of this assembly is an iron-dominated, superconducting magnet designed as a prototype objective lens for electron microscopy. The lens is formed by two identical iron yoke pieces containing both an axisymmetric pole region as well as a path for flux return outside of the coils. When assembled, the full gap of the sample region between pole pieces is 5 mm, and a 1.2 mm diameter hole for the beam tube passes through the yoke pieces to the sample region. A 280 turn coil of fine filament Nb-Ti superconducting wire developed for the SSC project [17] powers the magnet. The pole piece profile and axisymmetric magnetic field simulated using the commercial finite element analysis (FEA) software Opera3D are shown in figure 6. At the peak operating current of 30 A used for our studies, the lens gap field is 1.95 T and the calculated inductance is 5.54 mH.

A single-axis commercial hall probe (Lakeshore HGCT-3020) is located 1.9 mm offset from the center of the lens gap to measure the magnetic field in the direction crossing between the pole pieces. The probe is powered with a constant bias current of 25 mA using a Yokogawa GS200 DC source, and the voltage readout is performed using a Keithley 2182A nanovoltmeter which integrates over two power line cycles. The RMS voltage noise of this probe in liquid helium was evaluated as 10.7 nV using 10 minutes of 1 Hz data taken with the same equipment and in the same cryostat environment used for the experiment (without external field shielding). With the probe sensitivity of 95.8 mV/AT, this corresponds to a RMS field noise of 44.7 mG, which is roughly 2.5 ppm of the 1.77 T field at the hall probe location when the objective lens carries the nominal current of 30 A.

A pair of superconducting joints integrate the objective lens with an inductance tuner to create the closed superconducting circuit illustrated in figure 7 (a). A persistent current switch (PCS) shorts the two joints, allowing for the connection of resistive leads at the joint locations to initialize the persistent current with a power supply. The conceptual approach to the tuner design is shown in figure 7 (b). A superconducting coil is wound around an iron circuit containing two symmetric air gaps, resulting in a magnet for which the inductance is a strong function of the gap size. By mounting a portion of the iron circuit on a cryogenic stage, a re-positioning of the stage can be used to change the gap size and tune the inductance. The small tuner coil was wound with a magnet lead to avoid adding an additional superconducting joint to integrate the tuner in series with the objective lens. The tuner coil lead along with all other Nb-Ti wires were fixed to a G10 plate connected to the magnet structure to prevent movement.

To measure the yoke gap during operation, a set of cryogenic-compatible capacitive gap sensors from the commercial vendor Capacitec are included in the tuner assembly with location indicated in figure 5. In addition to the lens and tuner, the circuit also

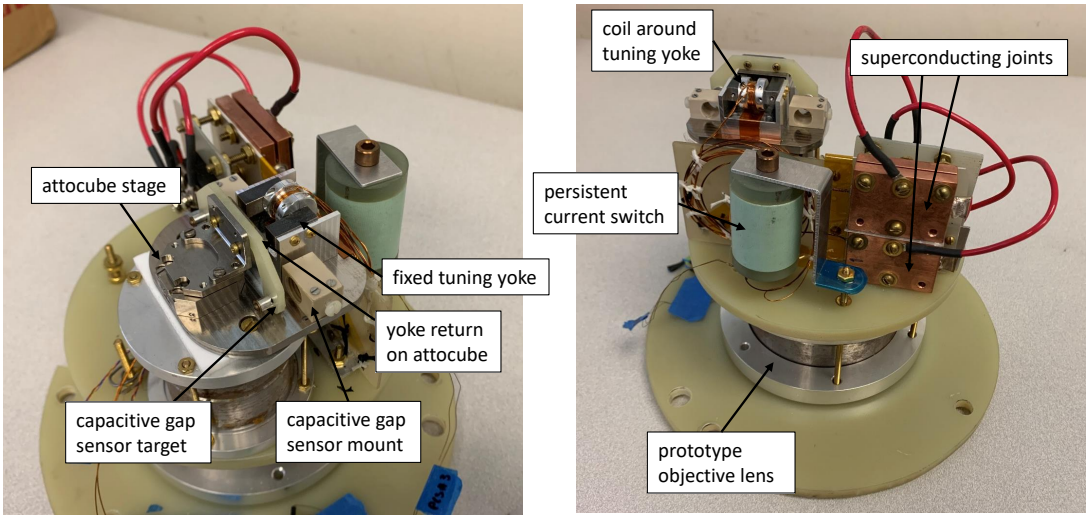

Figure 5. The magnet system consists of a 1.95 T prototype objective lens integrated with a movement-based flux tuner and persistent current switch using two superconducting joints.

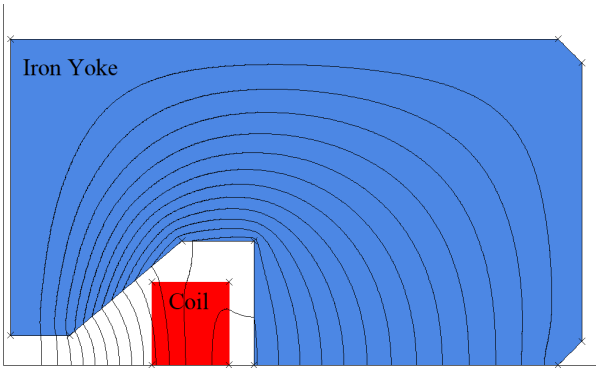

Figure 6. The iron and coil for a 2D symmetric region of the prototype objective lens with contours of the magnetic flux.

includes a superconducting transformer in series with the main lens (not shown in figure 7) for testing of other techniques not considered by this study. This adds a constant inductance of 9.4 μH to the circuit which has a negligible effect on the analysis.

To design a tuner for the objective lens, we first used an analytic approximation to establish the design variables and further to identify the range and boundaries of these parametric variables to explore with better accuracy using a FEA model (slow for evaluation). In the limits of infinite permeability in iron and small gap, the tuner design parameters can be reduced to the number of turns in the coil n, the cross-sectional area of a single pole a_{pole}, and the air gap size g. With these assumptions, the non-linear inductance of the tuner as a function of the gap is expressed as

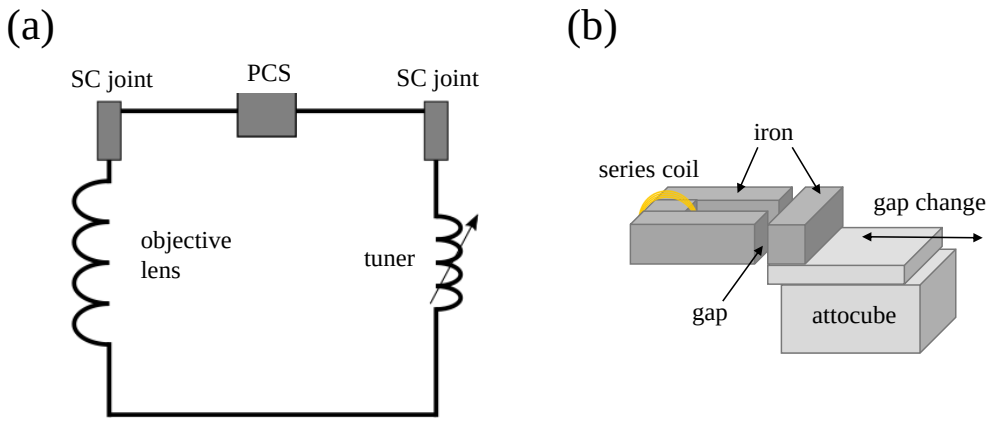

Figure 7. (a) Two superconducting joints create a closed superconducting loop with the objective lens and inductance tuner in series. (b) The inductance tuner consists of an iron circuit with adjustable air gap controlled by the attocube stage.

$$L_b(g) = \frac{\mu_0 n^2 a_{pole}}{2g}. \tag{12}$$

As discussed in section 2.2, key tuner design metrics are the total stabilization time and maximum deviation from the nominal current. If g_i and g_f mark the range over which the gap can be varied, the total amount of time over which the persistent current can be stabilized as a function of the joint resistance from equation 9, is

$$t_{stab} = -\frac{\mu_0 n^2 a_{pole}}{2R}\left(\frac{1}{g_f} - \frac{1}{g_i}\right). \tag{13}$$

Applying equation 6 to the infinite permeability and small gap model, the minimum relative current adjustment for a gap change step size of Δg, now a non-linear function of initial position g_0, is

$$\frac{\Delta i_{stab}}{i_0}(g_0) = \frac{L_b(g_0)}{L_m}\frac{\Delta g}{g_0}\left(1 + \frac{\Delta g}{g_0} + \frac{L_b(g_0)}{L_m}\right)^{-1} \tag{14}$$

The use of an attocube stage defines the resolution with which the gap can be adjusted as well as the total range over which the gap can be varied. Testing of the attocube ANP101x model in liquid helium showed a minimum repeatable step size of approximately 100 nm over the 5 mm range of total travel. Figure 8 shows contours of total stabilization as a function of the two free design parameters with an assumed circuit resistance of 10^{-11} Ω and initial gap of 0.5 mm. Because $\Delta i_{stab}/i_0$ is a function of the gap, the minimum deviation of current during the stabilization process is larger at the beginning of the stabilization than at the end (where the fixed 100 nm step results in a smaller current adjustment). For this reason, two sets of contours are included showing the stabilization time at the level of 10 and 1 ppb or less (which may only

include a portion of the total movement range). It is seen from figure 8 that there exists design choices which maximize the stabilization time for a given deviation. For a $\Delta i/i$ of 10^{-9} this maximum is between the 4 hour curves and for a $\Delta i/i$ of 10^{-8} the maximum is between the 36 hour contours.

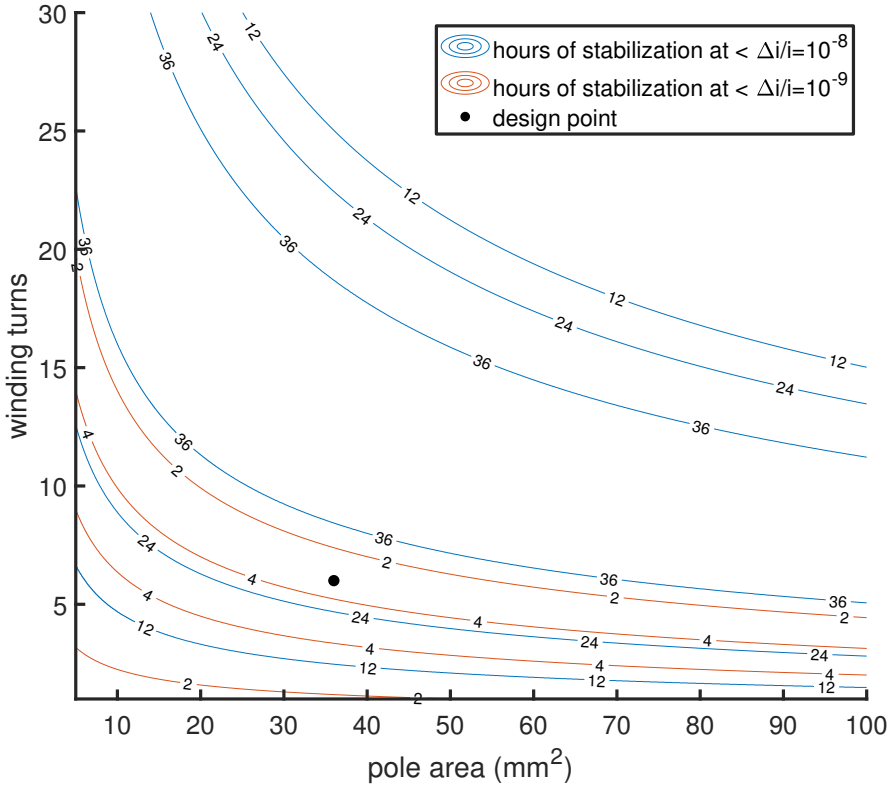

Figure 8. Contours of stabilization time versus tuner design parameters are shown for a circuit resistance of 10^{-11} Ω and minimum attocube step size of 100 *nm*. Two sets of contours mark the subset of the total stabilization time for which the theoretical deviation is kept less than 1 and 10 ppb.

The design point shown on figure 8 and described in table 1 was chosen as balance between longer stabilization at 10 ppb or greater and probing the limits of the design in the ppb or better regime. The results in table 1 are calculated using a FEA model for the tuner which includes effects of non-infinite permeability iron and the specific geometry of the tuner yoke and coil. For the inductance calculation, the current in the FEA model is perturbed by 0.5% from the operating current at which the inductance is desired. Then, the inductance is calculated from the resulting change in linked flux through the coil using $L = n\Delta\lambda/\Delta I$. For the chosen design parameters, this FEA calculation resulted in an inductance several times higher than predicted by the approximate analytical model. Figure 9 shows the calculated inductance of the tuner as a function of air gap at the nominal current of 30 A. For this figure, a group of FEA models are generated with geometry matching the range of gap values. Then, the perturbation method is applied to each of these models to evaluate the inductance for that specific gap.

Table 1. Overview of the tuner design

Parameter	Value	Unit
coil turns	6	
pole area	36	mm^2
minimum yoke gap	0.5	mm
maximum yoke gap	5.5	mm
max field at 30 A (at min gap)	0.16	T
max force at 30 A (at min gap)	700	mN
inductance at minimum gap	3.33	μH
inductance at maximum gap	2.22	μH
$\Delta i/i_0$ for 100 nm step (at min gap)	3.1×10^{-8}	
$\Delta i/i_0$ for 100 nm step (at max gap)	4.2×10^{-10}	
stab. time for R=10^{-11} Ω	31	hours
stab. time for R=10^{-11} Ω (at <1 ppb)	1.7	hours

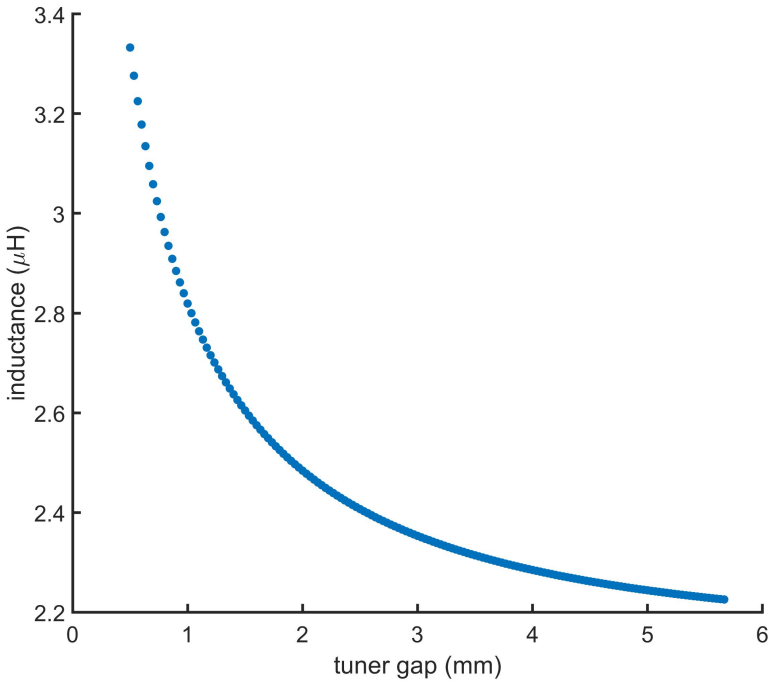

Figure 9. The inductance as a function of gap for the tuner magnet as calculated by the commercial FEA code Opera3D.

4. Experimental Demonstration

We report results from inductance tuning tests performed during persistent current operation at 30 A, corresponding to a magnetic field of 1.95 T in the gap of the main lens. For the expected behavior shown in sections 4.1 and 4.2, equation 2 is evaluated with the measured gap and tuner inductance from the FEA model (shown in figure 9). The level of field change resulting from inductance tuning in these tests is far greater than the observed resistive loss, allowing for the use of this no-loss predictive model. In section 4.3, the predicted tuner gap change as a function of time to stabilize the field is evaluated using equation 8, the previously mentioned FEA results for the tuner inductance as a function of gap, and the effective resistance calculated from the decay rate before and after the stabilization. At 30 A the lens is operating in a regime where the iron is partially saturated. For this reason, the local transfer function including saturation effects is used to convert changes in current predicted by the analytic model to predictions for the measured field. The FEA model also predicts a 7% drop in field from the center of the gap to the location of the hall probe. This is consistent with the field measured by the hall probe at 30 A of around 1.77 T.

4.1. Continuous current adjustment

To calibrate the persistent current tuner, we moved the attocube stage in the direction of increasing tuner gap at a constant rate of 4.6 $\mu m/s$. Figure 10 shows the change in measured field as a function of gap from 0.5 to 2.3 mm, which is roughly the range over which the capacitive gap sensors can measure. As expected, an increase in the tuner gap results in an increase of the persistent current, raising the field in the main lens. The measurements and calculated expected behavior are generally well matched, with both clearly showing the non-linearity of the tuning as a function of gap.

4.2. Step-based current adjustment

For this test, we adjusted the tuner gap outwards and back in steps of increasing size. Periods of no movement were included between steps in order to resolve the field level and noise. Figure 11 shows the measured gap and field as a function of time for two back-to-back tests with the same stage movement. The measured field clearly follows changes in the tuner gap and repeatability between runs is observed. In addition, the measured step changes in the field are in general agreement with the predicted values from the FEA calculation. Similar testing over a range of initial gap size was used to create a calibration table of stage movement and field change as a function of gap. This calibration allowed for determining the required stage movements during the automated field stabilization described in section 4.3. Step-based persistent current tuning demonstrates the ability to adjust the focal strength of the lens which is important during the initial setup and operation of the microscope.

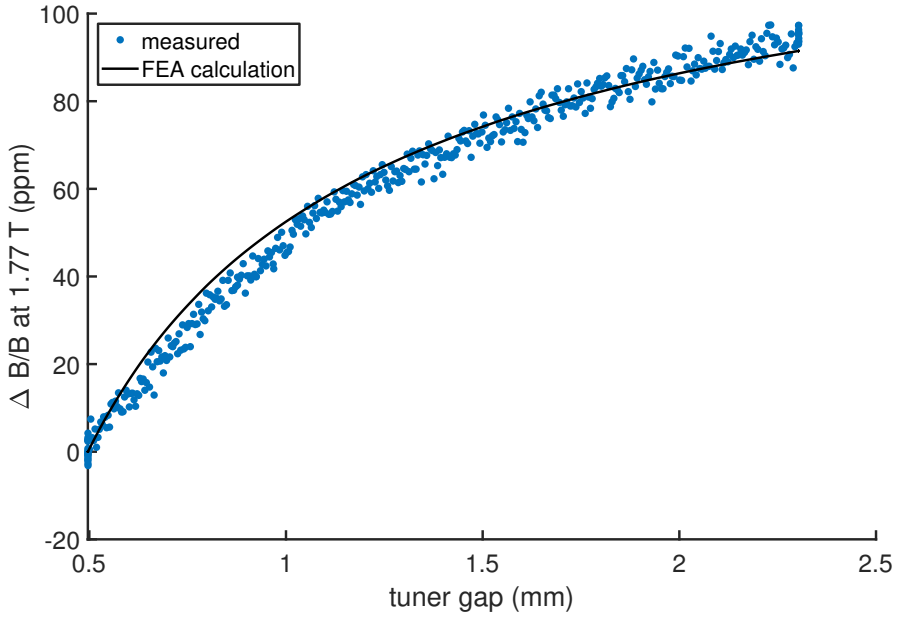

Figure 10. The measured change in main lens field as a function of tuner gap (controlled by the attocube stage) is compared to the expected non-linear behavior.

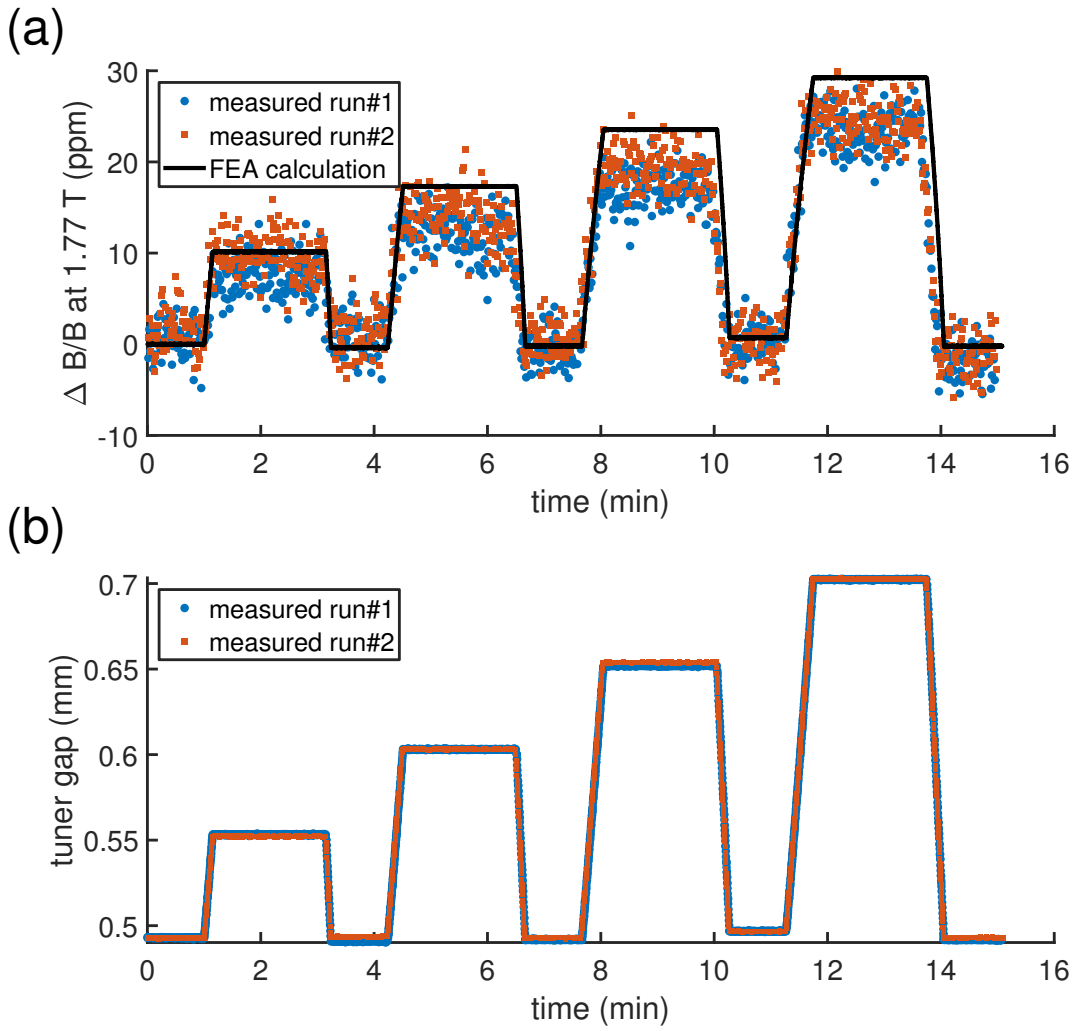

Figure 11. The measured field in the main lens (a) tracks changes in the tuner gap (b) for an increasing step pattern. The experiment is repeated twice, demonstrating repeatability and agreement with expected behavior.

4.3. Field stabilization

Figure 12 shows a typical magnet decay where we used inductance tuning to stabilize the field for a five hour period. After placing the magnet in persistent current mode, there is an initial fast decay which lasts for around one hour. Then, a second decay rate appears corresponding to an effective resistance ranging from 10 to 25 $p\Omega$. For this particular experiment, an initial test of the stabilization system perturbs the field in the region around two to four hours. Around eight hours after the magnet is placed into persistent current mode, an automated tuning program is started which uses magnetic field measurements as feedback to control the attocube stage and stabilize the field. After five hours, the stabilization program is ended and field continues to decay for a few more hours.

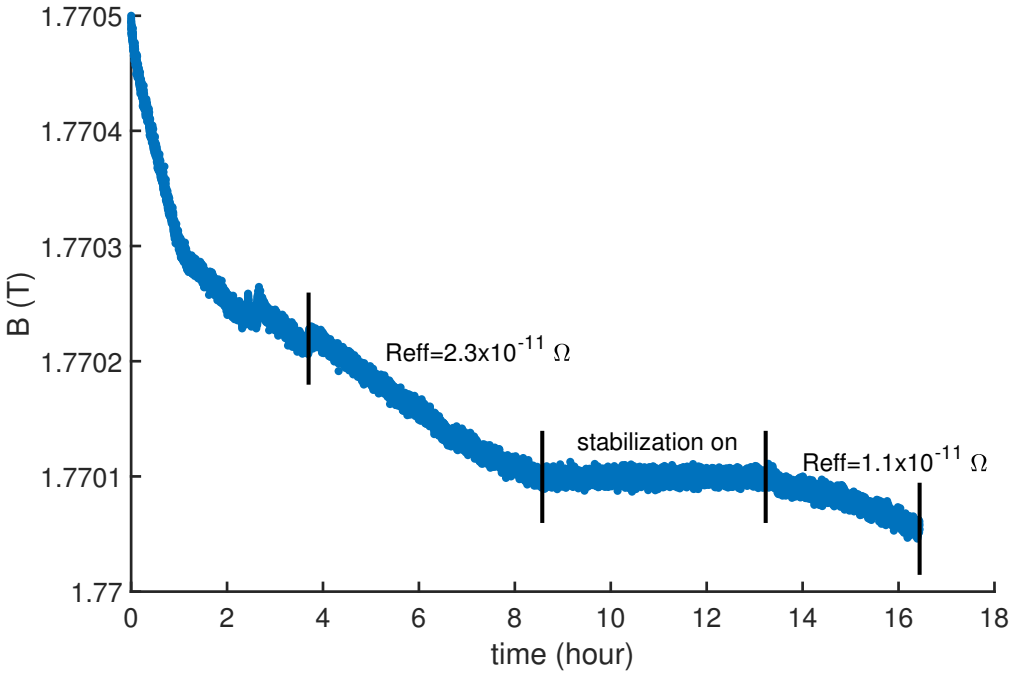

Figure 12. The measured field of the main lens in persistent current mode exhibits an initial regime of fast decay, followed by a regime with lower effective resistance. The disturbance in the field around 2-4 hours is due to a calibration of the tuning system. Four hours after this, the automated control software uses movement-based inductance tuning to stabilize the field for a period of five hours. Then, the control system is stopped and the field once again begins to decay.

The stabilization region is shown in more detail in figure 13. A setpoint for the field is created with reaction bounds of +/- 2.25 ppm. When the 18 second moving average of the field measured every 1.5 seconds crosses these bounds, a pre-determined adjustment of the tuner gap by the attocube is triggered. The scale of this adjustment is interpolated based on calibration runs similar to what is shown in section 4.2. In the bottom of figure 13, the tuner gap as a function of time is compared to the expected behavior calculated using the limiting cases of the decay rate before and after the stabilization program is

started. The expected behavior based on these limiting cases is seen mostly bounding the observed movements required to stabilize the field.

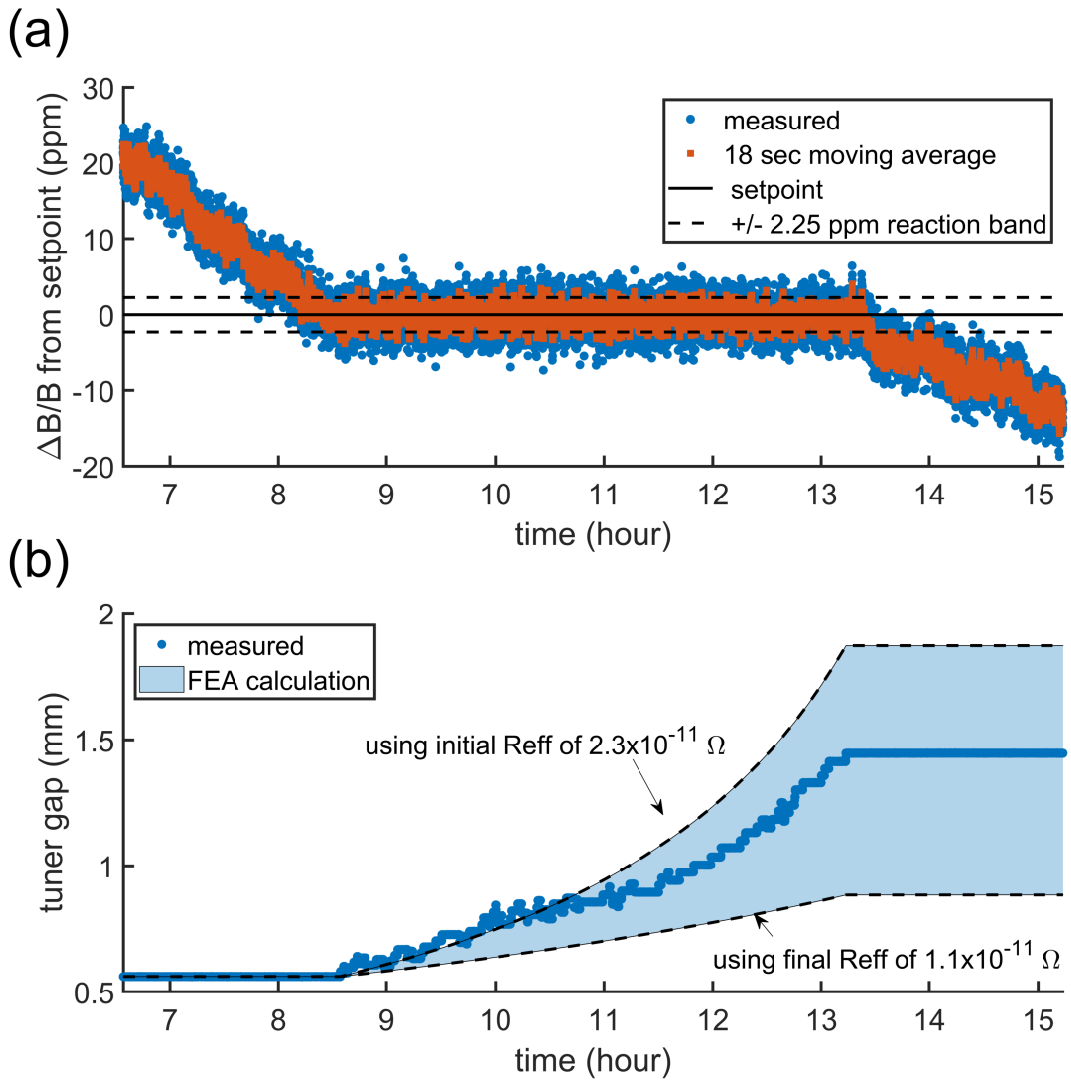

Figure 13. A detailed view of the stabilization region from figure 12 is shown in (a). A control software uses feedback from magnetic field measurements to trigger attocube stage movement and stabilize the magnetic field. When the moving average of the field crosses the reaction band, the stage moves a pre-calibrated distance to correct to the field drift back to the setpoint. The resulting movement of the stage is shown in (b), along with bounds of expected behavior calculated using the initial and final decay rates.

The choice of moving average (18 seconds) and reaction band (+/- 2.25 ppm) is a balance between triggering a current adjustment (attocube step) based on noise alone and minimizing deviation from the nominal current due to magnet decay. A longer moving average will reduce triggering an adjustment from noise, but will require a longer time to hit the reaction band that triggers a current adjustment due to lag in the average. For this experiment, we chose the initial size of the moving average and reaction band using a simulated noise model, then refined these values during a several

practice runs stabilizing the magnet in persistent current operation.

It is unknown why the decay rate is different before and after the period of active stabilization. The authors believe it is possible that this may be partially due to changes in the experimental environment such as the helium liquid level and temperature drift of the room temperature electronics powering and taking measurements from the hall probe. As described in section 5, future experiments will focus on understanding and eliminating environmental contributions to field drift and measurement accuracy.

5. Discussion of Results

We believe our experimental results demonstrate that: (1) inductance tuning is a viable method for adjustment and stabilization of the field in persistent current magnets, (2) the behavior is consistent with expectations derived from a very basic theory of flux conservation and loss in closed superconducting circuits, and (3) a 1.95 T round lens for electron microscopy can be stabilized at the level of several ppm. Our ability to demonstrate a greater degree of stabilization is limited by the noise level of the hall probe employed in our current experimental setup rather than limitations of the tuning system, which is designed with a theoretical reach of ppb level adjustments. When pushing towards the goal of ultra-precise tuning, it is expected that environmental stabilization and shielding not employed for this experiment are required. For these reasons, future experiments will focus on probing the stabilization limits of this setup with NMR or SQUID-based field measurement technology; superconducting shielding; and cryostat stabilization.

As described by equation 8, the inductance change required for field stabilization depends only on the total resistance of the circuit. We believe this gives direct relevance of our tuning device and results to the operation of MRI, NMR, or other persistent current magnets with superconducting joints of resistance near or less than the 10^{-11} Ω observed in our experiment. This level of resistance is typical of Nb-Ti to Nb-Ti joints created by the widely used solder replacement method. Contrary to the small, helium-filled space available for a field probe in the objective lens used for our current studies, many MRI magnets can readily accommodate field measurement based on NMR methods, enabling much finer field resolution (roughly 0.1 ppm). For this reason, testing of the inductance tuning concept with an MRI magnet is also a promising route to further probing the limits of the technique.

6. Conclusion

Inductance tuning in superconducting circuits allows for precise control and stabilization of superconducting magnets operating in persistent current mode. In this approach, extra flux stored in a tunable inductor at the point of initial powering is shifted to or from the main magnet by means of inductance change, enabling persistent current adjustment without the need for introducing new flux into the closed circuit. This decouples the speed and accuracy of current change from thermal processes typically required to break and close superconducting connections to add or remove flux. We apply the new technique to the operation of 1.95 T superconducting objective lens built as a prototype for electron microscopy. Tuning is realized by means of a small superconducting magnet with inductance dependent on the positioning of ferromagnetic material. Placing this material on a cryogenic stage couples movement of the stage to changes in persistent current. In a first set of experiments, we demonstrate stabilization and re-adjustment of the field in the objective lens at the level of several ppm, corresponding to the

noise limits of the cryogenic hall probes employed for field measurement. Future experiments will focus on probing the limits of the tuning setup, which is designed for ppb-level adjustments, with NMR or SQUID-based field measurement technology; superconducting shielding; and cryostat stabilization.

7. Acknowledgments

The authors thank Diego Arbelaez for guidance on capacitive gap sensors and Max Maruszewski, Tim Bogdanof, Jim Swanson, and Robert Memmo for technical support. This work was supported by the Director, Office of Science, Basic Energy Sciences, and U.S. Department of Energy under Contract No. DE-AC02-05CH11231. Work at the Molecular Foundry by authors P.E., A.M., C.O., and J.C. was also supported by the Office of Science, Office of Basic Energy Sciences, of the U.S. Department of Energy under Contract No. DE-AC02-05CH11231.

References

[1] Blaum K, Eliseev S and Sturm S 2021 *Quantum Sci. Technol.* **6** 014002
[2] Van Dyck R, Farnham D, Zafonte S and Schwinberg P 1999 *Rev. Sci. Instrum* **70** 1665
[3] Hanneke D, Fogwell S and Gabrielse G 2008 *Phys. Rev. Lett.* **100**(12) 120801
[4] Hanneke D, Fogwell S and Gabrielse G 2011 *Phys. Rev. A* **83** 052122
[5] J Repp et al 2012 *Appl. Phys. B* **107** 983–996
[6] F Heiße and S Rau and F Köhler-Langes and W Quint and G Werth and S Sturm and K Blaum 2019 *Phys. Rev. A* **100** 022518
[7] Brittles G D, Mousavi T, Grovenor C R M, Aksoy C and Speller S C 2015 *Supercond. Sci. and Technol.* **28** 093001
[8] Iwasa Y 2001 *Cryogenics* **41** 385–391
[9] Parizh M 2017 *Supercond. Sci. and Technol.* **30** 014007
[10] Moser E, Laistler E, Schmitt F and Kontaxis G 2017 *Frontiers in Physics* **5** 33
[11] Muller A and Grazul J 2001 *Journal of Electron Microscopy* **50** 219–226
[12] Haider M, Müller H, Uhlemann S, Zach J, Loebau U and Hoeschen R 2008 *Ultramicroscopy* **108** 167–178
[13] Lefranc G, Knapek E and Dietrich I 1982 *Ultramicroscopy* **10** 111–123 ISSN 0304-3991
[14] Gabrielse G and Tan J 1988 *J. Appl. Phys* **63** 5143
[15] Devlin J A, Wursten E, Harrington J A, Higuchi T, Blessing P E, Borchert M J, Erlewein S, Hansen J J, Morgner J, Bohman M A, Mooser A H, Smorra C, Wiesinger M, Blaum K, Matsuda Y, Ospelkaus C, Quint W, Walz J, Yamazaki Y and Ulmer S 2019 *Phys.Rev.Applied* **12** 044012
[16] Coombs T 2019 *Journal of Applied Physics* **125** 230902
[17] Teuho J, Erkolahti T, Haasjoki P, Lehto J, Liikamaa R and Vanhatalo V 1992 *Recent Results in Developing NbTi Fine Filament Superconductors* (Springer) ISBN 0198548052